AIAA Guidance, Navigation, and Control Conference and Exhibit
15 - 18 August 2005, San Francisco, California

AIAA 2005-6264

Flight Control and Simulation for Aerial Refueling

Atilla Dogan * and Shinya Sato †
Department of Mechanical and Aerospace Engineering
University of Texas at Arlington, TX 76019

William Blake ‡
Air Force Research Laboratory, Wright Patterson AFB OH 45433

This paper addresses the problem of controlling the receiver aircraft to achieve a successful aerial refueling. For the performance verification of the controller, a new set of nonlinear, 6-DOF, rigid body equations of motion for the receiver aircraft has been derived. The equations are developed using the reference frame as one that is attached to, translates and rotates with the tanker aircraft. Furthermore, the nonlinear equations contain the wind effect terms and their time derivatives to represent the aerodynamic coupling involved between the two aircraft. These wind terms are obtained using an averaging technique that computes the effective induced wind components and wind gradients in the receiver aircraft's body frame. Dynamics of the engine and the actuators are also included in the study. A linear position-tracking controller has been designed using a combination of integral control and optimal LQR design. The controller does not use the information of the tanker's vortex induced wind effects acting on the receiver aircraft as well as the mass change that occurs during refueling. The performance of the controller is evaluated in the high fidelity simulation environment employing the new sets of equations of motion. The simulation and control design are applied to a tailless fighter aircraft with innovative control effectors and thrust vectoring capability. Various allocation schemes for redundant control variables are analyzed in a realistic approach maneuver to the refueling contact position behind the tanker aircraft. In this paper, the performance evaluation is presented only during the initial phase of aerial refueling maneuver when the receiver aircraft maneuvers to reach the refueling contact position.

I. Introduction

Undoubtedly the most demanding and critical aircraft missions are those involving multiple vehicles and especially when they need to operate in close proximity with each other such as in formation flight and aerial refueling operations. Two of the most significant factors that affect the receiver's dynamics in an aerial refueling operation are the time-varying mass and inertia properties during fuel transfer, and the wind effect due to the tanker's trailing vortices. While the effect of the leader's vortices on the follower in a formation flight is beneficial in reducing drag/fuel consumed,[1] the influence of a tanker's vortices on a receiver aircraft during aerial refueling[2,3] can be detrimental to the stability of the receiver aircraft.

There has been some recent work[4–18] dealing with demonstration of the benefit of and issues with the control system development for aerial refueling. However, they do not study the effect of the tanker's trailing wake vortex on the receiver aircraft. Most of the previous work treat the vortex as an unknown disturbance or stochastic turbulence in the control law design procedure, and they do not attempt to verify their control design in an environment where the aircraft can be exposed to a realistic wake vortex. Since vortex–induced velocities acting on an aircraft are highly non-uniform, standard aerodynamic force and moment equations, based on airspeed, angles of attack and sideslip, and uniform wind components and gradients acting at the center of mass (CM) of the aircraft, cannot be used directly. To overcome this difficulty, there have been

*Member AIAA, Assistant Professor.
†Undergraduate student.
‡Associate Fellow AIAA, Aerospace Engineer.

Report Documentation Page

Form Approved
OMB No. 0704-0188

1. REPORT DATE	2. REPORT TYPE	3. DATES COVERED
AUG 2005		**00-00-2005 to 00-00-2005**

4. TITLE AND SUBTITLE	5a. CONTRACT NUMBER
Flight Control and Simulation for Aerial Refueling	5b. GRANT NUMBER
	5c. PROGRAM ELEMENT NUMBER
6. AUTHOR(S)	5d. PROJECT NUMBER
	5e. TASK NUMBER
	5f. WORK UNIT NUMBER
7. PERFORMING ORGANIZATION NAME(S) AND ADDRESS(ES) **Air Force Research Laboratory,Air Vehicles Directorate,Wright Patterson AFB,OH,45433**	8. PERFORMING ORGANIZATION REPORT NUMBER
9. SPONSORING/MONITORING AGENCY NAME(S) AND ADDRESS(ES)	10. SPONSOR/MONITOR'S ACRONYM(S)
	11. SPONSOR/MONITOR'S REPORT NUMBER(S)

12. DISTRIBUTION/AVAILABILITY STATEMENT
Approved for public release; distribution unlimited

13. SUPPLEMENTARY NOTES
The original document contains color images.

14. ABSTRACT

15. SUBJECT TERMS

16. SECURITY CLASSIFICATION OF:			17. LIMITATION OF ABSTRACT	18. NUMBER OF PAGES	19a. NAME OF RESPONSIBLE PERSON
a. REPORT **unclassified**	b. ABSTRACT **unclassified**	c. THIS PAGE **unclassified**		**15**	

two extreme approaches used thus far.[19–21] The first one is to generate a database of induced forces and moments for a specific pair of aircraft by very complicated CFD (Computational Fluid Dynamics) models or wind tunnel and/or flight test measurements. Obviously, the databases are extremely costly to generate, too computationally intensive to use for even near real–time simulation and very difficult to use in control system development. Furthermore, they are specific to certain pairs of aircraft and flight condition. Even in this case, incorporation of the nonuniform wind effect in the equations of motion as induced force and moment terms invalidates the definition of aero–related variables. For example, airspeed is the speed of the vehicle relative to the air and it is directly affected by the presence of wind, which is ignored when the effect of wind is only included as an additional force or moment. The other extreme is either to completely avoid modeling the effect of nonuniform wind and model it as an unknown disturbance or to model it in such a simplified manner that it is not reliable to use in verification work.

Recently, the authors have developed a novel modeling technique that enables the use of standard dynamic equations of motion and aerodynamic build-up equations with wind effect terms included.[3,22–28] First step is to derive the equations of motion of an aircraft in which the wind effect is explicitly stated under the assumption that the aircraft is is a uniform wind field, i.e. uniform wind components and uniform wind gradients. Since the vortex-induced wind field acting on the encountering aircraft is non-uniform in nature, the novel idea is to approximate the non-uniform induced wind components and gradients by equivalent uniform wind and gradients. Once a reasonable approximation is achieved, the implementation of aerodynamic coupling between aircraft flying in close proximity becomes far more direct and computationally efficient than the conventional procedure since the necessity for calculating the induced forces and moments during the simulation is overcome. This approach has been proven very useful and accurate in the case of formation flight modeling and control.[22–27]

In this paper, the same vortex effect modeling technique is applied to the aerial refueling problem. First, the equations of motion of the receiver aircraft are derived in terms of the position and orientation of the receiver relative to the tanker aircraft while the velocity vector of the receiver is represented as the sum of the velocity of the aircraft relative to the surrounding air and the velocity of the air relative to an inertial frame. Then, the full nonlinear equations of motion including the terms with translational and angular wind velocity components are implemented in a MATLAB/Simulink environment along with a vortex model employing the vortex effect modeling technique. The simulation model is developed specifically for a pair of tanker receiver aircraft: KC–135R as the tanker and a tailless fighter aircraft with innovative control effectors (ICE) and thrust vectoring.

For the receiver to track a commanded trajectory to approach the refueling contact position behind the tanker, a multi–input multi–output (MIMO) linear controller is designed and implemented in the simulation environment. The performance of the controller is evaluated in the simulation environment with the full nonlinear equations and trailing wake vortex from the tanker aircraft. Evaluation of the controller is carried out in three different allocation schemes of the redundant control variables: three control effectors, thrust magnitude and two thrust vectoring angles.

II. Modeling of the Receiver Dynamics Relative to the Tanker

In an efficient aerial refueling operation, the receiver aircraft needs to be controlled with respect to the tanker's position and orientation rather than with respect to an inertial reference. Additionally, the receiver aircraft will be exposed to a nonuniform wind field during the whole refueling operation when it is in the proximity of the tanker due to the trailing vortex of the tanker. Thus, a new set of nonlinear equations are derived[3] and used in this study to represent the position and orientation of the receiver relative to the tanker and at the same time to explicitly represent the vortex effect on the dynamics of the receiver aircraft.

A. Translational Kinematics and Dynamics

Since we are interested in the position of the receiver relative to the tanker and not its absolute position with respect to the ground, the translational kinematics equation is written in terms of the position vector of the receiver with respect to tanker (Fig. 1) :

$$\dot{\xi} = \mathbf{R_{B_R w_R}}\, V_w + W - \mathbf{R_{B_R B_T}} \mathbf{R_{B_T I}}\, \dot{r}_{B_T} + \mathbf{S}(\omega_{\mathbf{B_R B_T}} + \mathbf{R_{B_R B_T}} \omega_{\mathbf{B_T}})\xi \tag{1}$$

where ξ is the position of the receiver relative to the tanker expressed in the body frame of the tanker, $\mathbf{R_{B_R w_R}}$ is the rotation matrix from the receiver wind frame to body frame, V_w is the velocity of the receiver

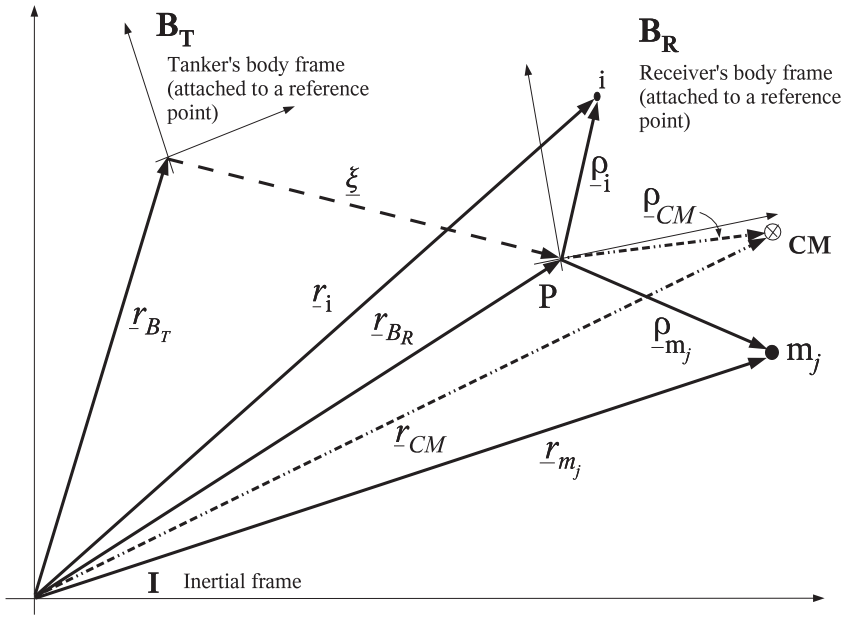

Figure 1. Intermediate reference frames: Tanker and Receiver's body frame

relative to the surrounding air expressed in the receiver wind frame, W is the velocity of the surrounding air relative to the ground expressed in the receiver body frame, $\mathbf{R_{B_R B_T}}$ is the rotation matrix from tanker body frame to receiver body frame, $\mathbf{R_{B_T I}}$ is the rotation matrix from the inertial frame to tanker body frame and $\dot{r}_{B_T}$ is the velocity of the tanker relative to the inertial frame. Also, note that $\mathbf{S}(\cdot)$ is the skew-symmetric operation on the representation of a vector and defined as

$$\mathbf{S}(x) = \begin{bmatrix} 0 & x_3 & -x_2 \\ -x_3 & 0 & x_1 \\ x_2 & -x_1 & 0 \end{bmatrix}, \tag{2}$$

for an arbitrary vector $\underline{x}$ with the representation $[x_1\ x_2\ x_3]^T$.

The equation of translational dynamics of the receiver aircraft including the wind effect, in matrix form, is given below:

$$\begin{aligned} \begin{bmatrix} \dot{V}_R \\ \dot{\beta}_R \\ \dot{\alpha}_R \end{bmatrix} &= \mathcal{E}_{\mathbf{R}}^{-\mathbf{1}} \Big[\mathbf{S}(\omega_{\mathbf{B_R B_T}}) + \mathbf{R}_{\mathbf{B_R B_T}} \mathbf{S}(\omega_{\mathbf{B_T}}) \mathbf{R}_{\mathbf{B_R B_T}}^{\mathbf{T}} \Big] \Big(\mathbf{R}_{\mathbf{B_R w_R}}\ V_w + W \Big) \\ &\quad - \mathcal{E}_{\mathbf{R}}^{-\mathbf{1}} \dot{W} + \frac{1}{m} \mathcal{E}_{\mathbf{R}}^{-\mathbf{1}} \Big(\mathbf{R}_{\mathbf{B_R B_T}} \mathbf{R}_{\mathbf{B_T I}} M_R + \mathbf{R}_{\mathbf{B_R w_R}}\ A_R + P_R \Big) \end{aligned} \tag{3}$$

where

$$\mathcal{E}_{\mathbf{R}}^{-\mathbf{1}} = \begin{bmatrix} \cos\alpha\cos\beta & \sin\beta & \cos\beta\sin\alpha \\ -\frac{1}{V_R}\cos\alpha\sin\beta & \frac{1}{V_R}\cos\beta & -\frac{1}{V_R}\sin\alpha\sin\beta \\ -\frac{1}{V_R}\sec\beta\sin\alpha & 0 & \frac{1}{V_R}\cos\alpha\sec\beta \end{bmatrix} \tag{4}$$

In this form of the translational equations, all the translational and rotational states of the receiver are with respect to the tanker body frame. Furthermore, the position vector is represented in the tanker body frame. Another advantage of this representation is due to the fact that the motion of the tanker aircraft - both translational and rotational - are passed as exogenous inputs to the receiver aircraft. The variables included in this category are velocity , $\dot{r}_{B_T}$, orientation in terms of euler angles ψ_T, θ_T, ϕ_T, and angular velocity p_T, q_T, r_T and translational velocity $\dot{r}_T$ of the tanker, all relative to the inertial frame.

The external forces acting on the receiver are the gravitational force vector $\underline{M}_R$ (expressed in the inertial frame), the aerodynamic force vector $\underline{A}_R$ (expressed in the wind frame of the receiver) and the propulsive force vector $\underline{P}_R$ (expressed in the body frame of the receiver). In general, the representations of the force vectors $\underline{M}_R$, $\underline{A}_R$ and $\underline{P}_R$ are

$$M_R = \begin{bmatrix} 0 \\ 0 \\ mg \end{bmatrix} \quad A_R = \begin{bmatrix} -D_R \\ -S_R \\ -L_R \end{bmatrix} \quad \underline{P}_R = \begin{bmatrix} T_x \\ T_y \\ T_z \end{bmatrix} \tag{5}$$

The propulsion force $\underline{P}_R$ has three components, which are functions of thrust magnitude T_R and the orientation of the thrust vector. The thrust vectoring is parameterized by the angle of the thrust vector with the receiver's body xy– and xz– planes. Thus, as seen in Fig. 2, the components of the thrust are

$$\begin{aligned} T_x &= T_R \cos\delta_z \cos\delta_y \\ T_y &= T_R \sin\delta_z \\ T_z &= T_R \cos\delta_z \sin\delta_y \end{aligned} \tag{6}$$

Note a positive δ_y rotation of the thrust generates a positive thrust component in the positive z–direction while inducing a positive pitching moment. Similarly, a positive δ_z rotation of the thrust generates a positive thrust component in the positive y–direction while inducing a negative yawing moment.

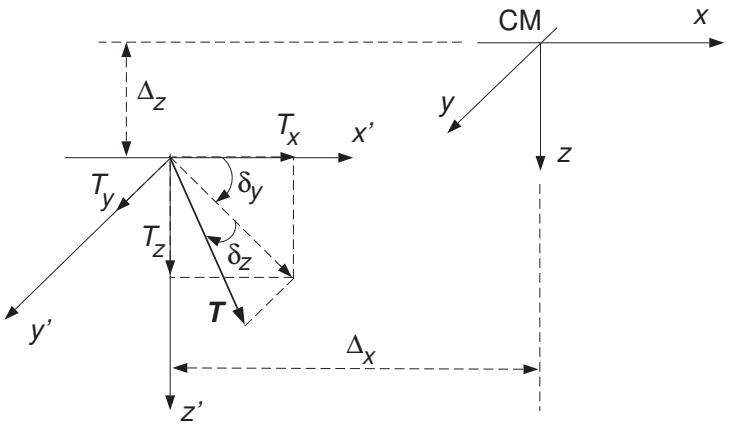

Figure 2. Thrust vectoring angles and moment arms

The aerodynamic forces are given by

$$D_R = \frac{1}{2}\rho V_R^2 \mathcal{S}_R C_D \ , \tag{7}$$

$$S_R = \frac{1}{2}\rho V_R^2 \mathcal{S}_R C_S \ , \tag{8}$$

$$L_R = \frac{1}{2}\rho V_R^2 \mathcal{S}_R C_L \ , \tag{9}$$

where $\mathcal{S}_R$ is the reference area of the receiver and ρ is the ambient air density. The aerodynamic coefficients are

$$C_D = C_{D0} + C_{D\alpha}\alpha + C_{D\alpha 2}\alpha^2 + C_{D\delta_e}\delta_e + C_{D\delta_e 2}\delta_e^2 \tag{10}$$

$$C_S = C_{S0} + C_{S\beta}\beta + C_{S\delta_a}\delta_a + C_{S\delta_r}\delta_r \tag{11}$$

$$C_L = C_{L0} + C_{L\alpha}\alpha + C_{L\alpha 2}(\alpha - \alpha_{ref})^2 + C_{Lq}\frac{c}{2V_R}q_{rel} + C_{L\delta_e}\delta_e \tag{12}$$

where α is the angle–of–attack, β is the side slip angle, q_{rel} is the angular velocity of the receiver relative to the surrounding air around the body–y axis and (δ_a, δ_e, δ_r) are the deflections of the control effectors (aileron, elevator, rudder) as the conventional control surfaces or (elevon, pitch flap, clamshell) as in the ICE (Innovative Control Effectors) aircraft, respectively.

B. Rotational Kinematics and Dynamics

The rotational motion of the receiver aircraft, similar to its translational motion, is also analyzed with reference to the tanker body frame. Even though the standard rotational kinematics and dynamics equations are used, their interpretations are different because both the angular position and velocity of the receiver aircraft are relative to the tanker body frame, an accelerating and rotating reference frame.

The rotational kinematics equation in the matrix form is the well known standard equation:

$$\mathbf{R_{B_R B_T}} \dot{\mathbf{R}}^{\mathbf{T}}_{\mathbf{B_R B_T}} = -\mathbf{S}(\omega_{\mathbf{B_R B_T}}) \ , \tag{13}$$

where $\omega_{B_R B_T}$ is the representation of the angular velocity vector of the receiver aircraft relative to the tanker body frame expressed in its own body frame as

$$\omega_{B_R B_T} = \begin{bmatrix} p_{R_T} \\ q_{R_T} \\ r_{R_T} \end{bmatrix} \tag{14}$$

The matrix form of the rotational dynamics of the receiver is also modeled with the standard rotational dynamics equation:

$$\dot{\omega}_{B_R B_T} = \underline{\mathbf{I}}^{-\mathbf{1}}_{\mathbf{R}} M_{B_R} + \underline{\mathbf{I}}^{-\mathbf{1}}_{\mathbf{R}} \mathbf{S}(\omega_{\mathbf{B_R B_T}} + \mathbf{R_{B_R B_T}} \omega_{\mathbf{B_T}}) \underline{\mathbf{I}}_{\mathbf{R}} \left(\omega_{B_R B_T} + \mathbf{R_{B_R B_T}} \omega_{B_T}\right) \tag{15}$$

where $\underline{\mathbf{I}}_{\mathbf{R}}$ is the inertia matrix of the receiver aircraft, M_{B_R} is the moment of the external forces around the origin of the receiver body frame and expressed in the receiver body frame as

$$M_{B_R} = \begin{bmatrix} \mathcal{L} \\ \mathcal{M} \\ \mathcal{N} \end{bmatrix} \tag{16}$$

. The moment has two main components; due to aerodynamic forces and due to the thrust, thus

$$\mathcal{L} = \frac{1}{2}\rho V_R^2 \mathcal{S}_R b C_{\mathcal{L}} - \Delta_z T_y + \Delta_y T_z \tag{17}$$

$$\mathcal{M} = \frac{1}{2}\rho V_R^2 \mathcal{S}_R c C_{\mathcal{M}} - \Delta_z T_x - \Delta_x T_z \tag{18}$$

$$\mathcal{N} = \frac{1}{2}\rho V_R^2 \mathcal{S}_R b C_{\mathcal{N}} - \Delta_y T_x + \Delta_x T_y \tag{19}$$

where b is the wingspan, c is the cord length of the receiver aircraft, and (Δ_x, Δ_y, Δ_z) are the moment arms of the thrust in the body frame of the receiver (see Fig. 2). The aerodynamic moment coefficients are

$$C_{\mathcal{L}} = C_{\mathcal{L}0} + C_{\mathcal{L}\delta_a}\delta_a + C_{\mathcal{L}\delta_r}\delta_r + C_{\mathcal{L}\beta}\beta + C_{\mathcal{L}p}\frac{b}{2V_R}p_{rel} + C_{\mathcal{L}r}\frac{b}{2V_R}r_{rel} \tag{20}$$

$$C_{\mathcal{M}} = C_{\mathcal{M}0} + C_{\mathcal{L}\alpha}\alpha + C_{\mathcal{L}\delta_e}\delta_e + C_{\mathcal{M}q}\frac{c}{2V_R}q_{rel} \tag{21}$$

$$C_{\mathcal{N}} = C_{\mathcal{N}0} + C_{\mathcal{N}\delta_a}\delta_a + C_{\mathcal{M}\delta_r}\delta_r + C_{\mathcal{N}\beta}\beta + C_{\mathcal{N}p}\frac{b}{2V_R}p_{rel} + C_{\mathcal{N}r}\frac{b}{2V_R}r_{rel} \tag{22}$$

where (p_{rel},q_{rel},r_{rel}) are components of the angular velocity of the aircraft relative to the surrounding air. When the aircraft is in a vortex field as in the case of tanker's trailing wake vortex field, these angular velocity components will be different from the angular velocity relative to the tanker of relative to the inertial frame. Their calculation will be explained in Section III. There will be some additional dynamics induced on the receiver due to the facts that the actual fuel transfer will in fact transfer momentum and that the inertia properties of the receiver aircraft will be time–varying. These additional dynamic effects –both translational and rotational – are not considered in the present study.

C. Engine Dynamics

The thrust generated by the engine (T) is

$$T = \xi \, T_{max} \tag{23}$$

where ξ denotes the instantaneous throttle setting and T_{max} is the maximum available thrust and assumed to be constant in this paper. The engine dynamics is modeled as that of a first order system with time constant τ. Therefore, we have

$$\dot{\xi} = \frac{\xi - \xi_t}{\tau} \ , \tag{24}$$

where ξ_t is the commanded throttle setting ($0 \leq \xi_t \leq 1$).

D. Actuator Dynamics

For the present study, only the actuator saturation and rate limit effects are considered. Other dynamics would be included in the future work. The deflection range attainable from the elevon is (-30 deg, 30 deg), from the pitch flap (-30 deg, 30 deg) and from the clamshells (0 deg, 60 deg). All the three control effectors have a rate limit of ±90 deg/sec. Likewise, the thrust vectoring has a limit of ± 30 deg in both directions and a rate limit of ±30 deg/sec.

III. Modeling the vortex and its effect

It is to be noted that the wind effect terms constituting the elements W, $\dot{W}$ in the receiver's equations of motion presented earlier are considered to be based on the uniform wind distribution acting at the receiver's CM, expressed in its body frame. But, the vortex-induced wind field acting on the receiver aircraft is non-uniform in nature. Therefore, to be able to use the standard aircraft equations of motion without doing any modifications, there is a need to approximate the non-uniform induced wind components and gradients by equivalent uniform wind and gradients. Once a fairly reasonable approximation can be achieved, the implementation of aerodynamic coupling between the tanker and the receiver becomes far more direct and computationally efficient than the conventional procedure which involves first the calculation of induced forces and moments from the wind distribution, and then inserting these forces and moments in the aircraft dynamics equations. The need for a simple and fairly accurate method of approximating the non-uniform vortex-induced wind field by its uniform equivalent forms the motivation for the material presented in this section.

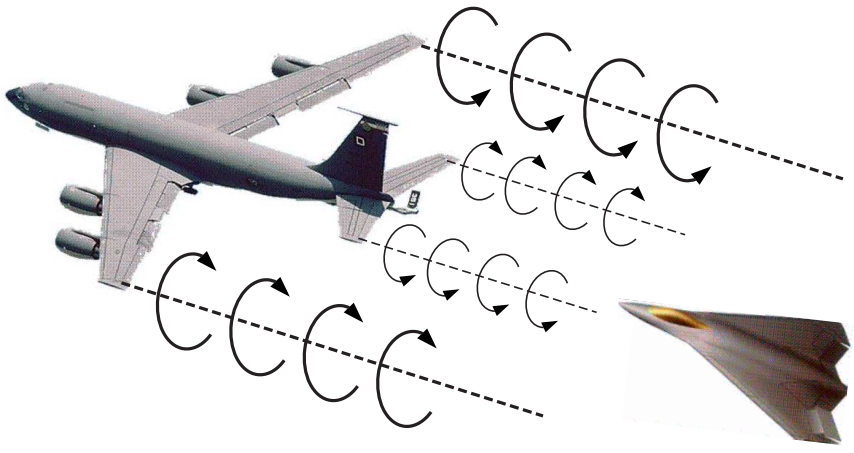

Figure 3. Trailing vortex from the wings and horizontal tail

In our dynamic model for aerial refueling, the tanker is considered to produce two pairs of straight, semi-infinite trailing vortex filaments – one from the wings and one from the horizontal tail – that induce additional wind velocities on the body of the receiver aircraft (see Fig. 3). These vortex-induced wind velocities cause changes in the forces and moments experienced by the receiver. However, instead of attempting to directly estimate the induced forces and moments on the follower, the induced wind velocities and wind gradients

are computed. The induced wind velocities are written as a function of the relative separation as well as the relative orientation between the tanker and the receiver using a modified horseshoe vortex model based on the Helmholtz profile. Since the induced wind and wind gradients are non-uniform along the body dimensions of the receiver aircraft, an averaging technique is implemented to compute the effective wind and wind gradient as uniform approximations. The effective wind components and gradients are introduced into the nonlinear aircraft equations that include the components of wind and the temporal variation of wind in the body frame to determine the effect on the receiver's dynamics. The effect of vortex decay over time is also included in our model. Special care has been taken to accommodate different geometrical dimensions for the tanker and the receiver aircraft and also to include many useful geometrical parameters of the aircraft like the wing sweep angle, the dihedral angle and the relative distance between the center of mass of the aircraft and the aerodynamic center of the wing, in estimating the vortex-effect experienced during aerial refueling. The previous publication[3, 22–28] of the authors should be referred to for further details of the actual vortex model and the averaging technique used to estimate the vortex-effect on the receiver.

IV. Control Design

Once the approach and fly-away trajectories are determined, a position-tracking controller is needed to make the receiver follow the reference trajectories. During the station-keeping phase of the refueling flight, the reference trajectory of the receiver is a constant with respect to the tanker's body frame. In the approach and fly-away maneuvers, the reference trajectories should be generated to ensure the overall safety of the receiver and the tanker. Therefore, it is very important to have a controller that can fly the receiver close to the reference trajectories.

The primary requirement of the control design is the tracking of the generated trajectories, with zero steady-state error in the x, y, z coordinates in the tanker's body frame, under the disturbance of trailing vortex, time variation of the inertia properties of the receiver and the possible steady maneuvers of the tanker's body frame. Meanwhile, the control inputs generated by the controller should not cause significant saturation on the magnitudes and rates of the actuators. Moreover, during the transient, overshoot or undershoot on trajectory response should be minimized to ensure the safety of the refueling. At the same time, the response of the closed loop system should be fast enough so that the approach and fly–away maneuvers are completed as planned and the high-wind regions of the trailing vortex field are exited in a timely fashion. Additionally, during the approach, fly–away and station-keeping maneuvers, the angle-of-attack and the airspeed should not be close to their corresponding stall values. In this regard, very big pitch angle should not be commanded. Finally, to ensure the safety of the aircraft, the bank angle should be small relative to its nominal value.

A combination of a multi–input multi–output LQR and integral control is employed in designing the position tracking controller satisfying the above requirements. First, the nominal conditions of the receiver aircraft are calculated at the steady level flight condition that the tanker is flying, i.e. the airspeed is equal to the tanker's speed, zero bank and zero yaw angles (recall that the euler angles are relative to the tanker) and zero side slip angle. Then, the nonlinear equations of motion of the receiver presented in Section II are linearized around this nominal condition. Note that in the linearization procedure, the wind terms are ignored while in the simulations the full nonlinear equations of motions are employed. The linearized equations of motion of the receiver in state-space form is obtained as

$$\dot{\underline{x}} = \mathbf{A}\underline{x} + \mathbf{B}\underline{u} + \mathbf{H}\underline{w} \tag{25}$$

where $\mathbf{A} \in \Re^{12\times12}$, $\mathbf{B} \in \Re^{12\times6}$, $\mathbf{H} \in \Re^{12\times6}$ (for the numerical values of the matrices, see Appendix A), the state vector is

$$\underline{x} = [\Delta V \;\; \Delta\beta \;\; \Delta\alpha \;\; \Delta p \;\; \Delta q \;\; \Delta r \;\; \Delta\psi \;\; \Delta\theta \;\; \Delta\phi \;\; \Delta x \;\; \Delta y \;\; \Delta z]^T \tag{26}$$

the control input vector is

$$\underline{u} = [\Delta\delta_a \;\; \Delta\delta_e \;\; \Delta\delta_r \;\; \Delta\xi \;\; \Delta\delta_y \;\; \Delta\delta_z]^T \tag{27}$$

and the disturbance vector due to the motion of the tanker is

$$\underline{u} = [\Delta V_{xT} \;\; \Delta V_{yt} \;\; \Delta V_{zT} \;\; \Delta\psi_T \;\; \Delta\theta_T \;\; \Delta\phi_T]^T \tag{28}$$

Since the position tracking controller is to be designed for the receiver relative to the tanker, the outputs

to be tracked are (Δx, Δy,Δz). Thus, output vector is chosen to be

$$\underline{y} = [\Delta x \ \ \Delta y \ \ \Delta z]^T \tag{29}$$

To ensure zero tracking error at steady state condition, the state space equations are augmented by three integrators, one for each position error:

$$\dot{\underline{e}} = \underline{y} - \underline{y_c} \tag{30}$$

where $\underline{y_c} = [\Delta x_c \ \ \Delta y_c \ \ \Delta z_c]^T$ is the commanded trajectory for the receiver in the body frame of the tanker for approaching the refueling contact position. Thus, in scalar form

$$\begin{aligned} \dot{e}_x &= \Delta x - \Delta x_c \\ \dot{e}_y &= \Delta x - \Delta x_c \\ \dot{e}_x &= \Delta x - \Delta x_c \end{aligned} \tag{31}$$

By including the augmentation states in the state–space equations, the augmented state equation becomes

$$\begin{bmatrix} \dot{x} \\ \dot{e} \end{bmatrix} = \begin{bmatrix} \mathbf{A} & \mathbf{0_{12\times 3}} \\ \mathbf{C} & \mathbf{0_{3\times 3}} \end{bmatrix} \begin{bmatrix} x \\ e \end{bmatrix} + \begin{bmatrix} \mathbf{B} \\ \mathbf{0_{3\times 6}} \end{bmatrix} \underline{u} + \begin{bmatrix} \mathbf{H} \\ \mathbf{0_{3\times 6}} \end{bmatrix} \underline{w} - \begin{bmatrix} \mathbf{0_{12\times 3}} \\ \mathbf{I_{3\times 3}} \end{bmatrix} \underline{y_c} \tag{32}$$

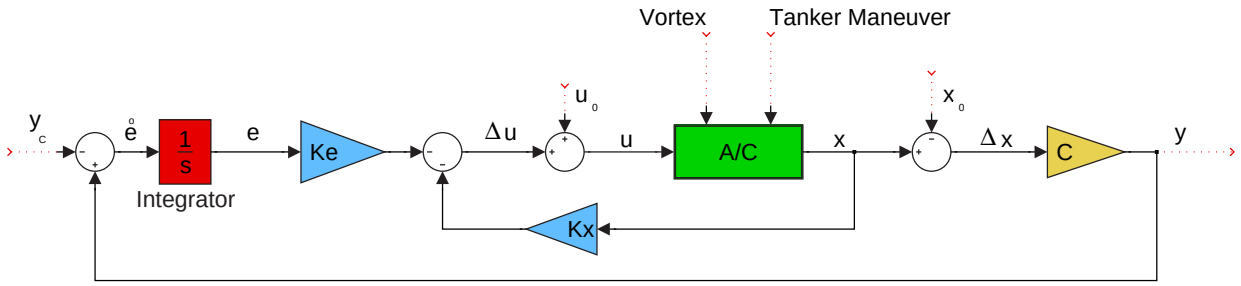

Figure 4. State feedback and integral control structure

Using LQR design technique, the state feedback gain matrix $[\mathbf{K_x} \ \mathbf{K_e}]$ is obtained to minimize the cost function:

$$J(\underline{u}) = \int_0^\infty \left\{ [\ \underline{x}^T \quad \underline{e}^T\ ] \mathbf{Q} \begin{bmatrix} \underline{x} \\ \underline{e} \end{bmatrix} + \underline{u}^T \mathbf{R}\, \underline{u} \right\} \mathrm{d}t \tag{33}$$

where $\mathbf{Q} \in \Re^{15\times 15}$ is symmetric positive semidefinite and $\mathbf{R} \in \Re^{6\times 6}$ is symmetric positive definite. Thus, the state feedback with the integral control is

$$\underline{u} = -\mathbf{K_x}\, \underline{x} - \mathbf{K_e}\, \underline{e} \tag{34}$$

V. Simulation Results

The Nonlinear equations of motion of the receiver are implemented in a MATLAB/Simulink–based model along with a tanker model. Both the receiver and the tanker models are equipped with their own controllers. The receiver controller is designed and implemented in such a way that various levels of control input allocations can be tested. The control variable allocation is achieved by varying the respective elements of the control weighting matrix $\mathbf{R}$ of the cost function in Eq. 33. Three different cases are simulated and compared in this section:

Case–1 : A combination of control effectors and thrust vectoring is used. $\mathbf{R}$ is chosen to a diagonal matrix with the following elements

$$\mathbf{R}(i,i) = (1, 1, 10, 1000, 50, 10) \tag{35}$$

Case–2 : Only control effectors are used without any thrust vectoring. $\mathbf{R}$ is chosen to a diagonal matrix with the following elements

$$\mathbf{R}(i,i) = (1, 1, 10, 1000, 1000000, 1000000) \tag{36}$$

Case–3 : Pitch Flap and Clamshell are fixed at their nominal values. Elevon and thrust vectoring are only control variables used. $\mathbf{R}$ is chosen to a diagonal matrix with the following elements

$$\mathbf{R}(i,i) = (10, 1000000, 1000000, 1000, 50, 100) \tag{37}$$

In all the three cases, $\mathbf{Q}$ is chosen to a diagonal matrix with the following elements

$$\mathbf{Q}(i,i) = 0.1 \times (1, 1, 1, 1, 1, 1, 1, 1, 1, 1, 0.001, 1, 1, 0.1, 1) \tag{38}$$

The refueling is performed at altitude of 7010 *meters* while the tanker is flying at speed of 200 m/sec. The simulations start when the receiver is laterally offset from the tanker by 60.96 *meters*, longitudinally 15.24 *meters* behind the refueling contact position and vertically at the same level as the the contact position. The refueling position is 25.33 *meters* directly behind and 6.46 *meters* below the c.g. of the tanker without any lateral offset. In other words, the receiver is initially at (-40.56,60.96,6.46) in the body–frame of the tanker and should go to and stay at (-25.33,0,6.46) for refueling . The receiver should move from the initial position to the refueling contact position by first maneuvering laterally right behind the tanker and then moving forward to the contact position without any altitude change (see Figs. 5 and 6).

Figure 5 shows the x– and y– components of both the commanded and actual trajectory of the receiver in the body frame of the tanker in case–1. Fig. 6 illustrates the x– , y– and z– components of the trajectory in time domain. As will be shown more clearly, when the simulation starts, the vortex-induced wind is not on and at 10 *seconds*, the wind is turned on and gradually increased to the normal level. This is done to ensure the start of the simulation without any numerical problem and also to see the effect of the vortex in the initial flight configuration. As seen Fig. 6, the lateral maneuver is initiated at around 50 *seconds* and lasts about a minute until the receiver is directly behind the tanker at 110 *seconds*. Then, at 125 *seconds*, the receiver starts moving forward towards and reaches the the refueling contact position in about 50 *seconds*. The trajectories of the other two cases are not presented because they all are similar to each other. Both the figures show that the commanded trajectories are closely tracked during the maneuver. Note that positive z–direction in down. Thus, the two spikes in the z–plot in Fig. 6 are in fact due to slight altitude lost first when the lateral maneuver starts and second when the forward motion is initiated.

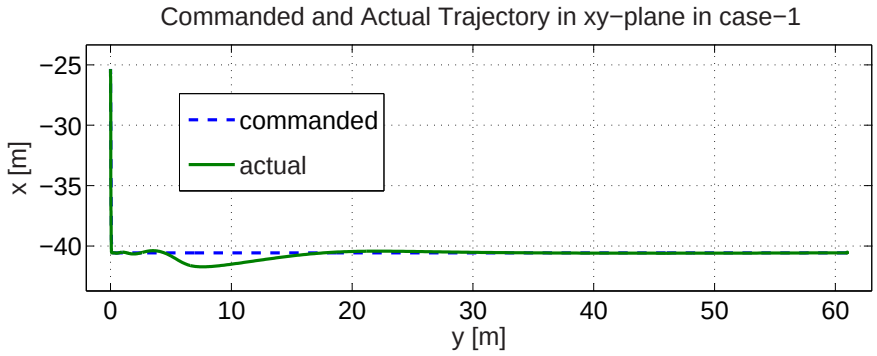

Figure 5. Trajectory of the receiver relative to the tanker in xy-plane

Figures 7,8 and 9 shows the initial levels of the control variables, how they vary during the entire maneuver and their final levels at the refueling positions in all the three cases. Fig. 7 illustrates the deflections of the three control effectors, elevon, pitch flap and clamshell. Note that the pitch flap and clamshell stay constant in case–3 because they are fixed at their nominal values. In all the three cases, very small deflections and deflection rates (much smaller than their respective saturation levels) in all the three effectors are used to move the receiver to the refueling position. Both elevon and clamshell, as expected, are mainly used during the lateral maneuver and stays almost constant during the forward motion. The behavior of the pitch flap

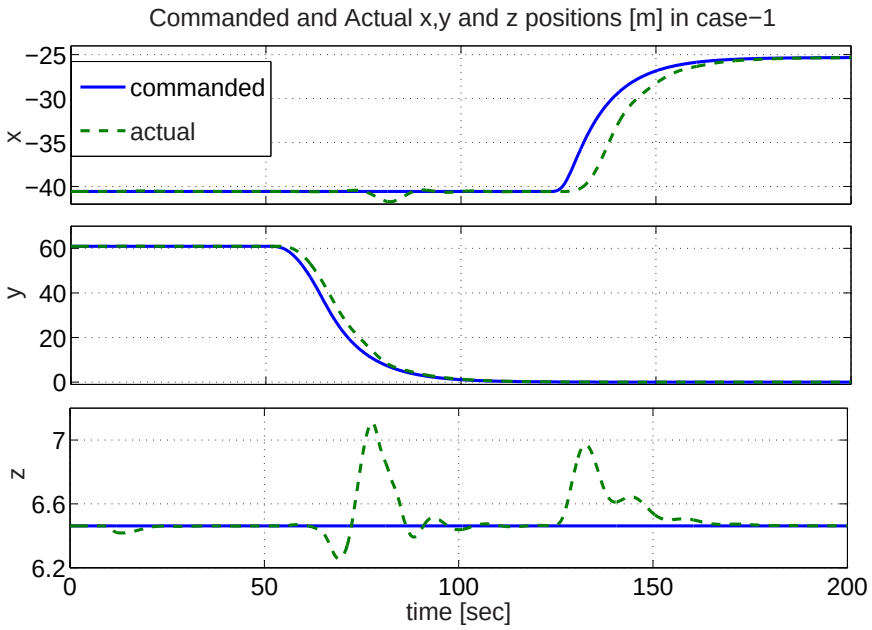

Figure 6. Commanded and actual x, y and z – positions of the receiver

is significantly different between case–1 and case–2. In case–2, it is used only during the lateral maneuver but in case–1 used in both lateral and forward maneuvers. This is because in case–1, it is coupled with the thrust vectoring as can be seen in Fig. 8.

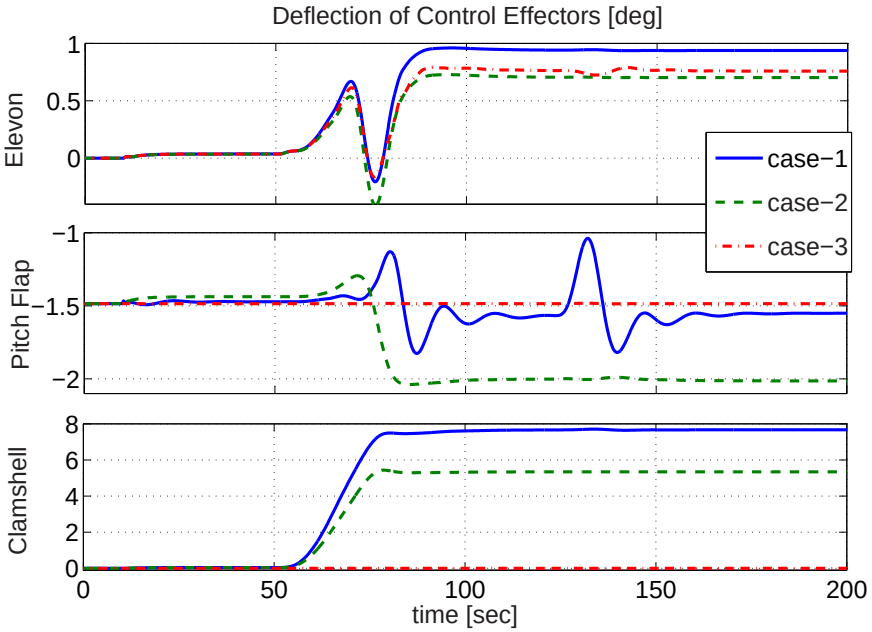

Figure 7. Deflections of the three control effectors in the three cases

Figure 8 shows the rotation of the thrust vector in terms of its angles with the xy– and xz– planes of the body–frame of the receiver. Note that rotation of angle with xy–plane induces pitching moment while generating vertical force. Similarly, rotation of angle with xz–plane induces yawing moment while generating lateral force. Also note that both the angles stay zero in case–2 since it represents no-thrust-vectoring configuration. In case–1, there is a direct correlation between angle with xy–plane and pitch flap since they

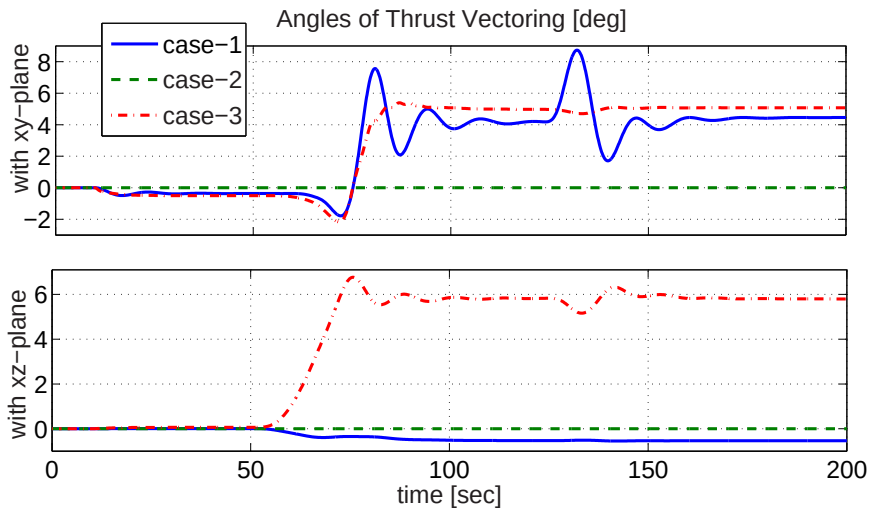

Figure 8. Thrust vectoring angle variation in the three cases

both mainly generate pitching moment. In case–3, since the pitch flap is fixed and thus no coupling, the angle with xy–plane increases during the lateral maneuver and stays at this new level afterwards. The angle with xz–plane in case–1 is decreased slightly while the clamshell angle is increased. However, in case–3, it is increased to about 6 *degrees* since the clamshell is not used at all. When the clamshell deflections in cases 1– and 2– are compared, it can be seen that its deflection is higher in case–1 and because it needs to compensates the moment induced by the rotation of the thrust by the negative angle with xz–plane.

Figure 9 illustrates the level of throttle in all the three cases. First note that when the vortex is turned on at 10 *seconds*, the level of throttle decreases slightly since the receiver aircraft is in the upwash region of the tanker's trailing vortex. During the maneuver in all the cases, the variation of the throttle setting is very similar. Once the receiver is at the refueling position, the throttle level in all the cases are much higher than that at the initial position. This is because at the final position, the aircraft is subject to strong downwash, which results in higher required thrust. The slight difference in the final level of throttle between the cases is due to the different thrust vectoring angles and different orientation of the aircraft at the refueling position.

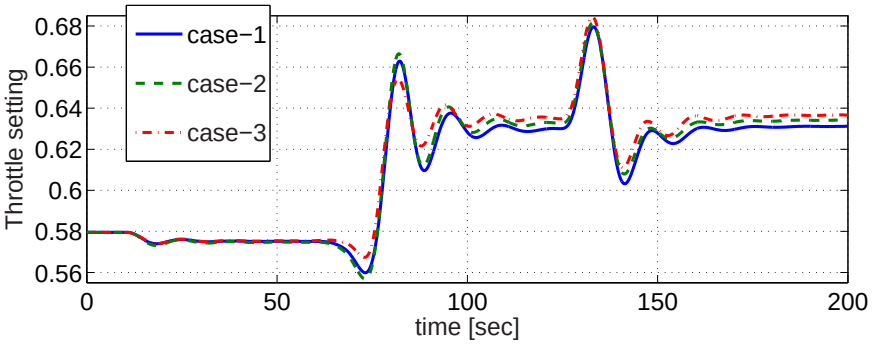

Figure 9. Variation in throttle level during the maneuver in the three cases

Figure 10 shows how the orientation of the receiver changes during the maneuvers in all the three cases in terms of euler angles relative to the tanker's body frame. Note that during the whole maneuver, all the euler angles are kept small by the controller while the position of the receiver aircraft changes and the level of vortex exposure increases. However, there is a nonzero yaw angle and it is not corrected by the controller in all the three cases. This is expected because the controller is designed to track the position with zero steady–state error by the additional integral controllers for the three commanded position signals while the LQR controller only guarantees the stability. However, three more integral control terms could be added to

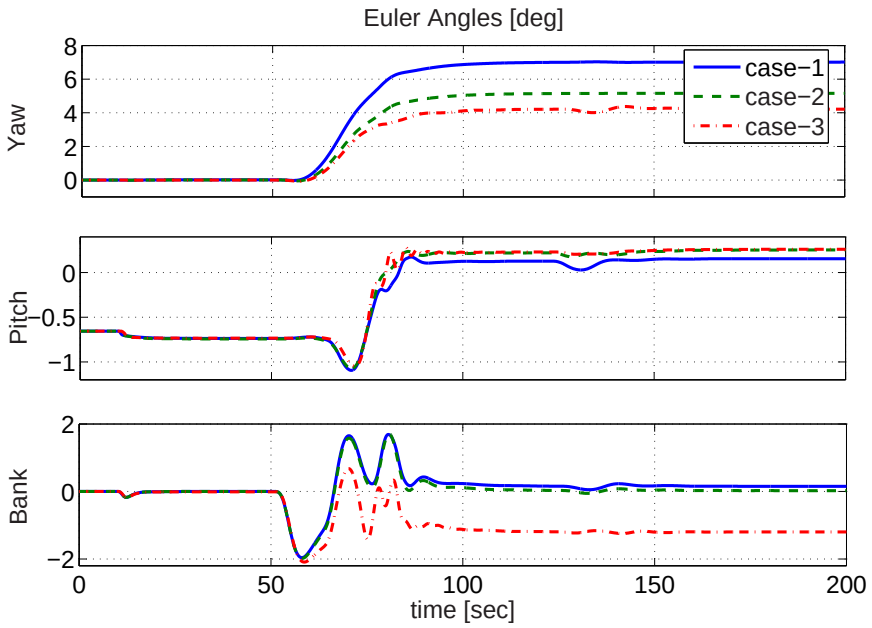

Figure 10. Orientation of the aircraft relative to the tanker in the three cases

the controller since there are six control variables in this receiver. Note that the final lateral equilibrium condition involves the highest yaw angle and clamshell deflection in case–1, slightly smaller ones in case–2 and smallest yaw angle while biggest thrust angle with xz–plane in case–3. On the other hand, there is a nonzero steady–state bank angle in case–3.

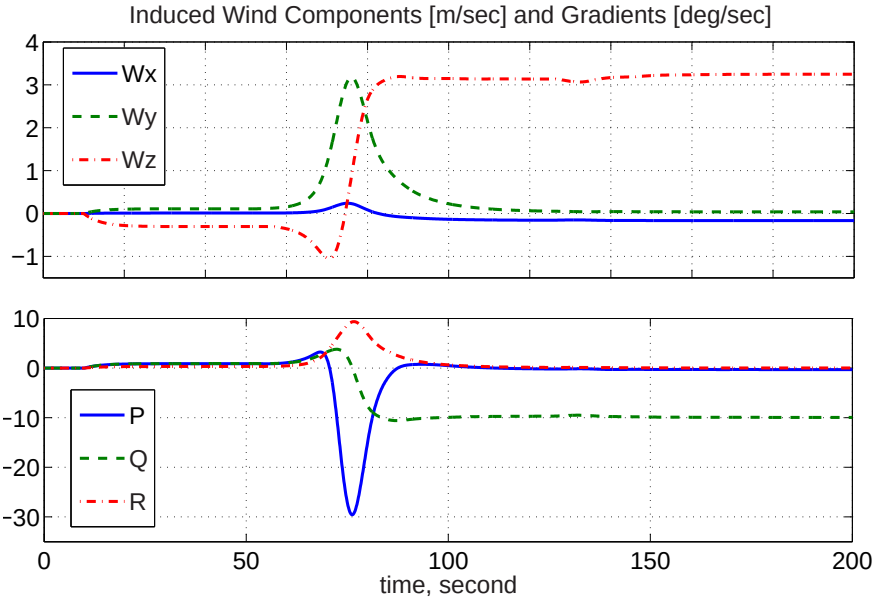

Figure 11. The wind components and gradients the receiver is exposed to in case–1

The vortex induced wind components and gradients are shown in Fig. 11 in case–1. In the other two cases the plots are similar. First note that at 10 *seconds*, the vortex is "turned on" and the aircraft is exposed to small upwash and sidewash and a slight "rolling" gradient. During the lateral maneuvers, as the receiver gets laterally closer to the tanker, both the amounts of effective wind components and gradients increases. At about 70 *seconds* when the lateral distance to the tanker is about %60 percent of the tanker's wingspan,

the highest upwash is experienced. As the receiver gets closer to the tanker when the lateral distance to the tanker is about %45 of the tanker's wingspan, the receiver experiences the greatest rolling vortex and the upwash turns into downwash while the sidewash increases dramatically. This is manifested in the rolling oscillation as seen in Fig. 10 and altitude drop in Fig. 6. During this transition, a yawing vortex gradient is experienced while a pitching gradient develops. As the receiver gets even closer to a position right behind the tanker, the rolling vortex gradient and sidewash disappear and downwash increases to its highest level. At the refueling contact position, two main vortex effect remains: strong downwash and pitching vortex gradient.

VI. Conclusion

In this paper, the equations of motion of a receiver aircraft are written in terms of its position and orientation relative to the tanker and its inertial velocity as the sum of its velocity relative to the surrounding air and the velocity of the air relative to an inertial frame. This enables the formulation of the relative motion of the receiver and facilitates the incorporation of the vortex induced wind effect into the translational and rotational equations of motion. Engine dynamics has been modeled as a first-order system. Saturation and rate limits are included in the model of actuator dynamics. An averaging technique has been outlined to incorporate the effects of the vortex-induced wind on the receiver's dynamics using the standard equations of motion. By this averaging technique, the non-uniform wind distribution induced by the vortex-field is approximated as uniform effective wind components and gradients acting at the receiver's CM.

A multi–input multi–output position-tracking state feedback controller is designed so that receiver aircraft tracks its reference trajectories specified in the tanker's body frame. To ensure zero steady–state error, the linearized equations of motion around the steady-level refueling flight condition are augmented with three integral states for the position tracking error in the three axes of the tankers body frame. The optimal LQR method is applied to the augmented system to obtain the constant gain matrix for state feedback and integral states. The controller is implemented in a MATLAB/Simulink–based simulation environment with the full 6–DOF nonlinear equations of motion for both the tanker and receiver including the wind terms as well as a vortex model employing an averaging technique to compute the effective translational and rotational wind velocities. The controller is not provided with the information of the trailing vortex.

The simulation and controller are applied to a pair of tanker-receiver aircraft: KC–135R and ICE aircraft (a tailless fighter aircraft with innovative control effectors and thrust vectoring capability). The performance of the controller is evaluated in the first phase of a refueling operation: the receiver aircraft starts away from the tanker and approaches the refueling contact position by tracking a commanded trajectory. Because of the redundancy of the control variables (6 control variables: three control effectors, thrust magnitude and two thrust vectoring angles), three control allocation scenarios are simulated: (1) combination of control effectors and thrust vectoring, (2) no thrust vectoring, and (3) pitch flaps and clamshells are fixed at their nominal values and thrust vectoring used for pitching and yawing moment generation. The simulation results show that the controller is capable of tracking the commanded trajectory without using the information of the nonuniform wind field in all the three control allocation schemes. However, at the contact position the steady state condition of the receiver may involve non–zero yawing angle and in the third case non–zero bank angle due to the vortex induced wind components and gradients. This will, in the next phase of this research work, be addressed by adding two more integral controls for the yaw and bank errors since there are enough number of control variables. The simulation is also proven to be a very realistic – at least qualitatively – evaluation environment to determine the effect of the trailing wake vortex on the receiver aircraft and to assess the performance of any aerial refueling controller. Another item of future work is to investigate the performance of the controller when the tanker aircraft is in a "racetrack" maneuver when the tanker starts to enter a turn with a max bank angle of 30 degrees, and holds this position until it is 180 degrees from its original heading, then it resumes straight flight. The receiver must be able to remain in the contact position with the boom connected throughout this maneuver. Moreover, in the vortex induced wind field, the stochastic content of the wind will be determined and modeled so that the performance of the controllers can be evaluated in the vortex induced wind field with turbulence.

References

[1]Blake, W. and Multhopp, D., "Design, Performance and Modeling Considerations for Close Formation Flight," *Proceedings of the 1998 AIAA GNC Conference*, Boston, MA, Jul. 1998, pp. 476–86, Paper no. 4343.

[2]Bloy, A. and Khan, M., "Modeling of the Receiver Aircraft in Air-To-Air Refueling," *AIAA Journal of Aircraft*, Vol. 38:2, 2001, pp. 393–396.

[3]Venkataramanan, S. and Dogan, A., "Dynamic Effects of Trailing Vortex with Turbulence & Time-varying Inertia in Aerial Refueling," *Proceedings of the AIAA Atmospheric Flight Mechanics Conference and Exhibit*, Providence, RI, August 2004, AIAA paper 2004-4945.

[4]Bloy, A. and Trochalidis, V., "Performance and longitudinal stability and control of large receiver aircraft during air to air refueling," *Aeronautical Journal*, Vol. 93:930, 1989, pp. 367–378.

[5]Bloy, A., West, M., Lea, K., and Jouma, M., "Lateral aerodynamics interference between tanker and receiver in air-to-air refueling," *Journal of Aircraft*, Vol. 30:5, 1993, pp. 705–710.

[6]Bloy, A. and West, M., "Interference between tanker wing wake with roll-up and receiver aircraft," *Journal of Aircraft*, Vol. 31:5, 1994, pp. 1214–1216.

[7]Bloy, A. and Jouma'a, M., "Lateral and directional stability and control in air-to-air refueling," *Proceedings of the Institution of Mechanical Engineers, Part G: Journal of Aerospace Engineering*, Vol. 209:4, 1995, pp. 299–305.

[8]Bloy, A. and Lea, K., "Directional stability of a large receiver aircraft in air-to-air refueling," *Journal of Aircraft*, Vol. 32:2, 1995, pp. 453–455.

[9]Pachter, M., Houpis, C., and Trosen, D., "Design of an air-to-air automatic refueling flight control system using quantitative feedback theory," *International Journal of Robust and Nonlinear Control*, Vol. 7:6, 1997, pp. 561–580.

[10]Pachter, M., Houpis, C., and Trosen, D., "Design of an Air-to-Air Automatic Refueling Flight Control System using Quantitative Feedback Theory," *Int. J. Robust Nonlinear Control*, Vol. 7, 1997, pp. 561–80.

[11]Coblei, B., "Capabilities and Future Applications of the NASA Autonomous Formation Flight (AFF) Aircraft," *1st AIAA UAV Conference*, Portsmouth, VA, May 2002.

[12]Valasek, J., Kimmett, J., Hughes, D., Gunnam, K., and Junkins, J., "Vision Based Sensor and Navigation System for Autonomous Aerial Refueling," *1st AIAA UAV Conference*, Portsmouth, VA, May 2002.

[13]Johnson, K. and Awni, K., "A Roll Autopilot for Autonomous Air Refueling," *AIAA Guidance, Navigation, and Control Conference and Exhibit*, Monterey, CA, Aug 2002.

[14]Fravolini, M., Ficola, A., Napolitano, M., Campa, G., and Perhinschi, M., "Development of Modelling and Control Tools for Aerial Refueling for Uavs," *AIAA Guidance, Navigation, and Control Conference and Exhibit*, Austin, TX, Aug 2003.

[15]Campa, G., Seanor, B., Perhinschi, M., Fravolini, M., Ficola, A., and Napolitano, M., "Autonomous Aerial Refueling for UAVs Using a Combined GPS-Machine Vision Guidance," *AIAA Guidance, Navigation, and Control Conference and Exhibit*, Providence, RI, Aug 2004.

[16]Lavretsky, V. S. E. and Hovakimyan, N., "Aerial Refueling Autopilot Design Methodology: Application to F-16 Aircraft Model," *AIAA Guidance, Navigation, and Control Conference and Exhibit*, Providence, RI, Aug 2004.

[17]Hansen, J., Murray, J., and Campos, N., "The NASA Dryden AAR Project: A Flight Test Approach to an Aerial Refueling System," *AIAA Atmospheric Flight Mechanics Conference and Exhibit*, Providence, RI, Aug 2004.

[18]Bennington, M. A. and Visser, K. D., "Aerial Refueling Implications for Commercial Aviation," *AIAA Journal of Aircraft*, Vol. 42:2, 2005, pp. 366–375.

[19]Jewell, W. and Stapleford, R., "Mathematical Models used to Simulate Aircraft Encounters with Wake Vortices," *STI Technical Report 1035-4*, 1975, pp. 38–57.

[20]Pachter, M., D'Azzo, J., and Proud, A., "Tight Formation Flight Control," *J. Guidance, Control, and Dynamics*, Vol. 24:2, 2001, pp. 246–254.

[21]Johnson, W., Teper, G., and Rediess, H., "Study of Control System Effectiveness in Alleviating Vortex Wake Upsets," *J. Aircraft*, Vol. 11, no.3, 1974, pp. 148–154.

[22]Dogan, A. and Venkataramanan, S., "Nonlinear Control for Reconfiguration of Unmanned–Aerial–Vehicle Formation," *AIAA Journal of Guidance, Control and Dynamics*, Vol. 28:4, Jul–Aug 2005, pp. 667–678.

[23]Dogan, A., Venkataramanan, S., and Blake, W., "Modeling of Aerodynamic Coupling Between Aircraft in Close Proximity," *AIAA Journal of Aircraft*, Vol. 42:4, Jul–Aug 2005, pp. 941–955.

[24]Venkataramanan, S. and Dogan, A., "Modeling of Aerodynamic Coupling Between Aircraft in Close Proximities," *Proceedings of the AIAA Atmospheric Flight Mechanics Conference and Exhibit*, Providence, RI, Aug 2004, AIAA paper 2004-5172.

[25]Venkataramanan, S. and Dogan, A., "A MultiUAV Simulation for Formation Reconfiguration," *Proceedings of the AIAA Modeling and Simulation Technologies Conference and Exhibit*, Providence, RI, August 2004, AIAA paper 2004-4800.

[26]Venkataramanan, S., Dogan, A., and Blake, W., "Vortex Effect Modelling in Aircraft Formation Flight," *Proceedings of the AIAA Atmospheric Flight Mechanics Conference and Exhibit*, Austin, TX, August 2003, AIAA paper 2003-5385.

[27]Venkataramanan, S. and Dogan, A., "Nonlinear Control for Reconfiguration of UAV Formation," *Proceedings of the AIAA Guidance, Navigation, and Control Conference*, Austin, TX, Aug. 2003, AIAA paper 2003-5725.

[28]Venkataramanan, S., *Dynamics and Control of Multiple UAVs Flying in Close Proximity*, M.S. Thesis, The University of Texas at Arlington, Arlington, TX, 2004.

A. State, Control and Disturbance Matrices

The state matrix of the linearized equations of motion at the steady–level flight condition:

$$\mathbf{A} = \begin{bmatrix}
-0.0189 & 0 & 5.6614 & 0 & 0 & 0 & 0 & -9.8066 & 0 & 0 & 0 & 0 \\
0 & 0.0027 & 0 & 0.0371 & 0 & -0.9993 & 0.0024 & 0 & 0.0490 & 0 & 0 & 0 \\
-0.0005 & 0 & -0.8286 & 0 & 0.9869 & 0 & 0 & 0 & 0 & 0 & 0 & 0 \\
0 & -6.9501 & 0 & -1.4768 & 0 & 0.1092 & 0 & 0 & 0 & 0 & 0 & 0 \\
0.0004 & 0 & -2.1237 & 0 & -1.5508 & 0 & 0 & 0 & 0 & 0 & 0 & 0 \\
0 & -1.7038 & 0 & -0.0477 & 0 & -0.0217 & 0 & 0 & 0 & 0 & 0 & 0 \\
0 & 0 & 0 & 0 & 0 & 1.0001 & 0 & 0 & 0 & 0 & 0 & 0 \\
0 & 0 & 0 & 0 & 1.0000 & 0 & 0 & 0 & 0 & 0 & 0 & 0 \\
0 & 0 & 0 & 1.0000 & 0 & -0.0115 & 0 & 0 & 0 & 0 & 0 & 0 \\
0.9988 & 0 & -9.7144 & 0 & 0 & 0 & 0 & 9.7144 & 0 & 0 & 0 & 0 \\
0 & 200.0000 & 0 & 0 & 0 & 0 & 199.7639 & 0 & -9.7144 & 0 & 0 & 0 \\
0.0486 & 0 & 199.7639 & 0 & 0 & 0 & 0 & -199.7639 & 0 & 0 & 0 & 0
\end{bmatrix}$$

The control matrix of the linearized equations of motion at the steady–level flight condition:

$$\mathbf{B} = \begin{bmatrix}
0 & 1.0160 & 0 & 3.2642 & 0.0703 & 0 \\
0 & 0 & 0 & 0 & 0 & 0.0095 \\
0 & -0.2328 & 0 & -0.0006 & 0.0095 & 0 \\
-41.2203 & 0 & -1.2436 & 0 & 0 & 0.1362 \\
0 & -14.9545 & 0 & -0.0748 & 1.3937 & 0 \\
-1.2203 & 0 & -1.4814 & 0 & 0 & -0.9981 \\
0 & 0 & 0 & 0 & 0 & 0 \\
0 & 0 & 0 & 0 & 0 & 0 \\
0 & 0 & 0 & 0 & 0 & 0 \\
0 & 0 & 0 & 0 & 0 & 0 \\
0 & 0 & 0 & 0 & 0 & 0 \\
0 & 0 & 0 & 0 & 0 & 0
\end{bmatrix}$$

The disturbance matrix of the linearized equations of motion at the steady–level flight condition:

$$\mathbf{H} = \begin{bmatrix}
0 & 0 & 0 & 0 & -9.8066 & 0 \\
0 & 0 & 0 & 0 & 0 & 0.0490 \\
0 & 0 & 0 & 0 & 0 & 0 \\
0 & 0 & 0 & 0 & 0 & 0 \\
0 & 0 & 0 & 0 & 0 & 0 \\
0 & 0 & 0 & 0 & 0 & 0 \\
0 & 0 & 0 & 0 & 0 & 0 \\
0 & 0 & 0 & 0 & 0 & 0 \\
0 & 0 & 0 & 0 & 0 & 0 \\
-0.9988 & 0 & 0.0486 & 0 & 9.7144 & 0 \\
0 & -1.0000 & 0 & 200.0000 & 0 & -9.7144 \\
-0.0486 & 0 & -0.9988 & 0 & -199.7639 & 0
\end{bmatrix}$$